Coupled Electro-Thermal Transient Analysis of Superconducting DC Transmission Systems Using FDTD and VEM Modeling

Dimitrios I. Doukas, *Member, IEEE*, Andreas I. Chrysochos, *Member, IEEE*, Theofilos A. Papadopoulos, *Member, IEEE*, Dimitris P. Labridis, *Senior Member, IEEE*, Lennart Harnefors, *Fellow, IEEE*, and Giovanni Velotto

***Abstract*—In this paper, detailed mathematical formulation of a coupled electro-thermal model for transient studies of high-temperature superconducting (HTS) transmission systems is presented. Regarding the thermal modeling, the volume-element method is used in order heat transfer equations on a two-dimensional axisymmetric cable model to be solved and temperature distribution over space and time to be determined. For the modeling of the electric part, a constant-parameter finite-difference time-domain method is utilized to calculate voltages and currents over space and time as well. The analysis is conducted on a bipolar cable suggested by the Electric Power Research Institute for long-distance HTS dc transmission to highlight the electric and thermal domain interaction under transient conditions. Different test cases are conducted to evaluate the electric and thermal transient performance of the examined HTS cable.**

***Index Terms*—Coupled electro-thermal modeling, finite-difference time-domain (FDTD), superconducting transmission, transients, volume-element method (VEM).**

I. Introduction

RECENT technological advances, especially on converter topologies, enabled dc transmission to emerge as a competitor to ac solution, especially for high-capacity power transmission with numerous advantages, such as increased controllability and bidirectional power transfer capability [1]. In parallel, the discovery of high-temperature superconductivity [2] was a breakthrough that made feasible the combination of such advantages with an almost lossless transmission system that utilizes high-temperature superconducting (HTS) cables [3]. Although several HTS transmission projects can be found around the world, either on laboratory level or in real-grid applications [4], technical obstacles preventing their massive adoption within the modern power grid exist. Issues such as their cost, the overall complexity, and the cooling-system reliability need to be considered [5]. Taking into account the rarity of experimental installations and lab prototypes, design and analysis of large-scale superconducting equipment on a modeling/simulation basis becomes more important [6]–[8]. Detailed mathematical formulations and robust/reliable computational tools combined with time-efficient solvers are needed to define an operation framework for both steady-state and transient conditions. Hence, dealing with complex, typically coupled magneto-thermal [9], electro-thermal [10], or mechanical-thermal [11] problems of applied superconductivity becomes feasible.

A literature survey on coupled electro-thermal modeling for HTS cables revealed several recent attempts. In [12], a code that focuses on the coupled thermal-hydraulic electromagnetic problem of the current and temperature distribution was presented. The role of thermal-hydraulics on the interpretation of the conductor test via the self-consistent computation of temperature profiles along and across the conductor combined with the voltage evolution was addressed, while the results were also experimentally validated. Moreover, in [9], a finite element model (FEM) of an HTS cable was built considering current and heat transfer boundary conditions, in order to simulate the magnetic-thermal coupled field. Focus was given on obtaining thermal stability of the HTS cable under different operating conditions. Furthermore, in [10], a three-dimensional coupled electro-thermal model of an HTS cable, developed in FEM was presented to determine the current sharing temperature of the cable and to study the quench phenomena that may occur. Lastly, in [13], a time-frequency domain reflectometry (TFDR) method was proposed to protect operational failures of grid-connected HTS cables. The cryogenic system and the status of the grid-connected HTS cable were both monitored via TFDR in a real-time manner.

Regarding transient analysis of HTS dc cables, in [14] and [15], parameters that influence the transient voltage distribution

Manuscript received March 23, 2017; revised September 3, 2017; accepted September 3, 2017. Date of publication September 6, 2017; date of current version September 22, 2017. The work of A. I. Chrysochos was conducted in the framework of the act "Support of Post-Doc Researchers" under the Operational Program "Human Resources Development, Education and Lifelong Learning 2014–2020," which is implemented by the State Scholarships Foundation and co-financed by the European Social Fund and the Hellenic Republic. This paper was recommended by Associate Editor C. Luongo. *(Corresponding author: Dimitrios Doukas.)*

D. I. Doukas, A. I. Chrysochos, and D. P. Labridis are with the School of Electrical and Computer Engineering, Aristotle University of Thessaloniki, Thessaloniki 54124, Greece (e-mail: doux@auth.gr; anchryso@auth.gr; labridis@auth.gr).

T. A. Papadopoulos is with the Power Systems Laboratory, Department of Electrical and Computer Engineering, Democritus University of Thrace, Xanthi 67100, Greece (e-mail: thpapad@ee.duth.gr).

L. Harnefors and G. Velotto are with the ABB Corporate Research, Västerås 72178, Sweden (e-mail: lennart.harnefors@se.abb.com; giovanni.velotto@se.abb.com).

Color versions of one or more of the figures in this paper are available online at http://ieeexplore.ieee.org.

Digital Object Identifier 10.1109/TASC.2017.2749500

along the cable and electrical transients that may lead to permanent damage were discussed, respectively. Moreover, characteristics under fault conditions for copper and HTS cables were compared in [16]. More recently, in [17] and [18], detailed transient thermal analysis of HTS dc cables was presented and system contingencies in which the system undergoes a transition that may lead to quenching were studied. Finally, thermo-electric responses in the cases of transients, thermal stability, and quench behavior were studied in [19].

The scope of this paper is to present an efficient methodology for the simulation of coupled electro-thermal transients for HTS dc cables. The volume-element-method (VEM) discretization technique is combined with FDTD, to analyze the coupled electro-thermal transient performance of HTS cables. The flexible parabolic-elliptic partial differential equations (PDEPE) solver [20] of MATLAB [21] is used to calculate the temperature profile for all cable layers over varying time and space. Heat transfer by conduction, convection, and radiation is considered. FDTD is adopted as a discretization technique to calculate voltages and currents at different cable segments, thus combined with VEM enables the simultaneous solution of the coupled electro-thermal problem.

The proposed methodology is generalized and can be used as a simulation and design tool to analyze any HTS cable configuration. The proposed model predicts the electric and thermal behavior under various transient conditions and can be useful to identify a secure operation framework.

In Section II, the thermal problem formulation and VEM analysis are presented. In Section III, the electrical problem formulation and FDTD modeling are given. In Section IV, the electro-thermal coupling is described. Sections V and VI focus on the case study and the results for various transients, respectively. Finally, Section VII concludes the paper.

II. Thermal Formulation and VEM Analysis

Thermodynamics and heat transfer laws are expressed by partial differential equations (PDEs) written in the generic form of (1). PDEs are introduced into PDEPE solver of MATLAB, which deals with initial-boundary value problems for varying space z and time t

$$c\left(z,t,T,\frac{\partial T}{\partial z}\right)\frac{\partial T}{\partial t}=z^{-m}\frac{\partial}{\partial z}\left[z^{m}f\left(z,t,T,\frac{\partial T}{\partial z}\right)\right]+s\left(z,t,T,\frac{\partial T}{\partial z}\right). \tag{1}$$

All PDEs hold for $t_0 \le t \le t_f$ and $a \le z \le b$, where t_0 and t_f represent the start and end time of simulation, while a and b represent the sending and receiving end of the HTS cable. Superscript m corresponds to symmetry and can be 0, 1, or 2 for slab, cylindrical, or spherical symmetry, respectively. Considering the numerical solution of (1), it is important to define the vector functions of flux $f(z,t,T,\frac{\partial T}{\partial z})$ and source $s(z,t,T,\frac{\partial T}{\partial z})$ terms. The coupling of the partial derivatives with respect to time is restricted by multiplying with a diagonal matrix $c(z,t,T,\frac{\partial T}{\partial z})$, with diagonal elements either zero for elliptic equations or positive for parabolic equations [20].

Initial conditions for the simulation starting at $t = t_0$ and for all z, i.e., over the whole cable length, are given by

$$T(z,t_0)=T_0(z). \tag{2}$$

Boundary conditions for all t and for one of the cable terminations, a or b, are determined by (3) and are expressed in terms of the flux term f. Therefore, two boundary conditions are introduced for the whole timespan, one for $z = a$ and one for $z = b$. Vector functions p and q are both time and space dependent, whereas only p may also depend on T. The elements of q are either identically zero or never zero

$$p(z,t,T)+q(z,t)f\left(z,t,T,\frac{\partial T}{\partial z}\right)=0. \tag{3}$$

Scalars z and t are considered as inputs, while vectors T and $\frac{\partial T}{\partial z}$ represent the solution T and its partial derivative with respect to z, respectively. The solution T for the thermal problem is the temperature distribution for varying space and time. PDEPE calculates temperature distribution over space and time for all finite volume elements (VEs) of any cable layer. As initial conditions in this work, the temperature at $t = t_0$ and for all z is considered for all cable layers.

VEM analysis divides cable layers in finite VEs using cylindrical coordinates for simultaneous discretization over space and time. Energy equations in terms of thermodynamics and heat transfer are solved in order to identify the variation of properties, such as temperature, over the cable length, and time. The analysis that follows results in a system of PDEs, representing heat transfer between VEs in r and z directions.

Heat transfer by conduction, convection, and radiation is considered. The discretization approach as well as the heat transfer model expressed by (4)–(10) are based in the analysis of [4], [22]. Note that the flux term f and source term s of (1) represent heat transfer on z and r directions, respectively.

A. Conduction

Between two consecutive VEs of solid materials, heat transfer by conduction on both radial and axial directions takes place. The expressions for heat conduction in $i-1$, i, and $i+1$ consecutive VEs of the lth layer are given in (4). Note that all VEs consist of the same material with thermal conductivity k_l and a cross-section $A_{r,l}$ on the z direction

$$\begin{cases}\dot{Q}^{i}_{l,\mathrm{d,in}}=-\frac{k_l A_{r,l}(T^{i}_{l}-T^{i-1}_{l})}{\Delta^{i-1}_{z}}\\ \dot{Q}^{i}_{l,\mathrm{d,out}}=-\frac{k_l A_{r,l}(T^{i+1}_{l}-T^{i}_{l})}{\Delta^{i+1}_{z}}.\end{cases} \tag{4}$$

Similarly, the expressions for heat conduction for consecutive VEs of the ith cross section of the cable between different l_1 and l_2 cable layers on r direction are given by

$$\dot{Q}^{i}_{l_1 l_2,\mathrm{d}}=U^{i}_{l_1 l_2}(T^{i}_{l_2}-T^{i}_{l_1}) \tag{5}$$

while $U^{i}_{l_1 l_2}$ is

$$U^{i}_{l_1 l_2}=\left(\frac{\ln\frac{2R_{l_1}}{R_{l_1-1}+R_{l_1}}}{2\pi k_{l_1}\Delta^{i}_{z}}+\frac{\ln\frac{R_{l_1}+R_{l_2}}{2R_{l_1}}}{2\pi k_{l_2}\Delta^{i}_{z}}\right)^{-1} \tag{6}$$

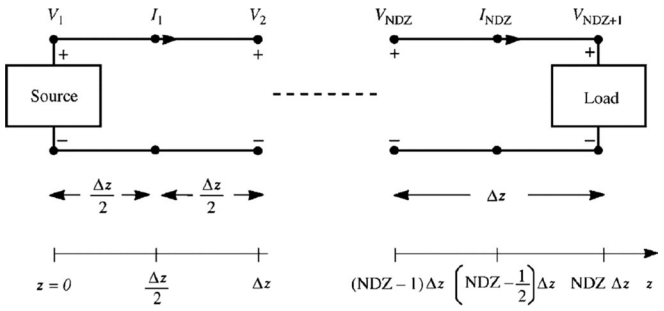

Fig. 1. Line discretization for the FDTD analysis [23].

where R_{l_1}, R_{l_2}, and R_{l_1-1} are the radii of layers l_1, l_2, and of the inner layer before l_1, respectively.

B. Convection

Heat transfer by convection might also exist on both r and z directions between solid and liquid materials. For mass flow $\dot{m}_l$ and specific heat c_{p_l}, heat convection for consecutive VEs on z and r directions is given by (7) and (8), respectively

$$\begin{cases} \dot{Q}^i_{l,\mathrm{v,in}} = -\dot{m}_l c_{p_l}(T^i_l - T^{i-1}_l) \\ \dot{Q}^i_{l,\mathrm{v,out}} = -\dot{m}_l c_{p_l}(T^{i+1}_l - T^i_l) \end{cases} \tag{7}$$

$$\dot{Q}^i_{l_1 l_2,\mathrm{v}} = h_{l_1} A^i_{l_1,l_2}(T^i_{l_2} - T^i_{l_1}) \tag{8}$$

where for Nusselt number Nu and hydraulic diameter D_h, h_{l_1} equals

$$h_{l_1} = \frac{k_{l_1}\mathrm{Nu}}{D_h}. \tag{9}$$

C. Radiation

Heat radiation occurs outside the cryogenic enclosure, where vacuum is imposed. Given that A^i_l corresponds to the cylindrical surfaces, heat radiation for consecutive VEs of the ith line cross section between different l_1 and l_2 cable layers, that surround vacuum layer, on the r direction is given by

$$\begin{cases} \dot{Q}^i_{\mathrm{r,in}} = -\frac{\varepsilon_{l_1}}{1-\varepsilon_{l_1}} A^i_{l_1}\left[B_1 - \sigma(T^i_{l_1})^4\right] \\ \dot{Q}^i_{\mathrm{r,out}} = -\frac{\varepsilon_{l_2}}{1-\varepsilon_{l_2}} A^i_{l_2}\left[\sigma(T^i_{l_2})^4 - B_2\right] \end{cases} \tag{10}$$

where σ is the Stefan–Boltzmann constant, ε is the material emissivity and B_1 and B_2 are determined in [22].

III. Electrical Formulation and FDTD Modeling

In FDTD formulation, the lossy multiconductor transmission line representation is used [23], as shown in Fig. 1. Specifically, constant parameter FDTD is used to reduce simulation time, while ensuring that transient results are on the safe side. The line is divided into NDZ sections, each of fixed length Δz, and the total solution time into NDT segments of fixed length Δt. The solution starts with an initially relaxed line of zero voltage and current values.

Step 1: Voltages along the line are calculated in terms of the past solutions, for a fixed time step Δt and n time instants

$$\mathbf{V}^{n+1}_k = \left(\frac{\Delta z}{\Delta t}\mathbf{C} + \frac{\Delta z}{2}\mathbf{G}\right)^{-1}\left(\frac{\Delta z}{\Delta t}\mathbf{C} - \frac{\Delta z}{2}\mathbf{G}\right)\mathbf{V}^n_k - \left(\frac{\Delta z}{\Delta t}\mathbf{C} + \frac{\Delta z}{2}\mathbf{G}\right)^{-1}\left(\mathbf{I}^{n+1/2}_k - \mathbf{I}^{n+1/2}_{k-1}\right) \tag{11}$$

for $k = 2, 3, \ldots, \mathrm{NDZ}$.

Step 2: Terminal conditions at HTS ends are incorporated using (12) and (13) to determine the corresponding voltages and currents, i.e., V_1, I_1, and $V_{\mathrm{NDZ}+1}$, I_{NDZ}.

$$\mathbf{V}^{n+1}_1 = \left(\frac{\Delta z}{\Delta t}\mathbf{R}_\mathrm{S}\mathbf{C} + \frac{\Delta z}{2}\mathbf{R}_\mathrm{S}\mathbf{G} + \mathbf{1}_n\right)^{-1}\left[\left(\frac{\Delta z}{\Delta t}\mathbf{R}_\mathrm{S}\mathbf{C} - \frac{\Delta z}{2}\mathbf{R}_\mathrm{S}\mathbf{G} - \mathbf{1}_n\right)\mathbf{V}^n_1 - 2\mathbf{R}_\mathrm{S}\mathbf{I}^{n+1/2}_1 + \left(\mathbf{V}^{n+1}_\mathrm{S} - \mathbf{V}^n_\mathrm{S}\right)\right] \tag{12}$$

$$\mathbf{V}^{n+1}_{\mathrm{NDZ}+1} = \left(\frac{\Delta z}{\Delta t}\mathbf{R}_\mathrm{L}\mathbf{C} + \frac{\Delta z}{2}\mathbf{R}_\mathrm{L}\mathbf{G} + \mathbf{1}_n\right)^{-1}\left[\left(\frac{\Delta z}{\Delta t}\mathbf{R}_\mathrm{L}\mathbf{C} - \frac{\Delta z}{2}\mathbf{R}_\mathrm{L}\mathbf{G} - \mathbf{1}_n\right)\mathbf{V}^n_{\mathrm{NDZ}+1} + 2\mathbf{R}_\mathrm{L}\mathbf{I}^{n+1/2}_{\mathrm{NDZ}} + \left(\mathbf{V}^{n+1}_\mathrm{L} - \mathbf{V}^n_\mathrm{L}\right)\right]. \tag{13}$$

Step 3: Currents are calculated by means of the calculated voltages and past current values

$$\mathbf{I}^{n+3/2}_k = \left(\frac{\Delta z}{\Delta t}\mathbf{L} + \frac{\Delta z}{2}\mathbf{R}\right)^{-1}\left(\frac{\Delta z}{\Delta t}\mathbf{L} - \frac{\Delta z}{2}\mathbf{R}\right)\mathbf{I}^{n+1/2}_k - \left(\frac{\Delta z}{\Delta t}\mathbf{L} + \frac{\Delta z}{2}\mathbf{R}\right)^{-1}\left(\mathbf{V}^{n+1}_{k+1} - \mathbf{V}^{n+1}_k\right) \tag{14}$$

for $k = 1, 2, \ldots, \mathrm{NDZ}$.

Given w is the number of conducting layers, $\mathbf{C}$, $\mathbf{G}$, $\mathbf{L}$, and $\mathbf{R}$ are $w \times w$ matrices, representing the per-unit length capacitance, conductance, inductance, and resistance matrices of the transmission line [23], [24], at the frequency of interest [25]. $\mathbf{1}_n$ corresponds to the identity matrix of the same order.

To ensure stability, space and time discretization must satisfy the Courant Friedrichs Lewy (CFL) [26] condition. For a stable solution, the CFL condition suggests that the time step must not exceed the observed propagation time along one Δz

$$\Delta t \leq \frac{\Delta z}{u}. \tag{15}$$

IV. Electro-Thermal Coupling

For all cable segments considered from the VEM analysis, the corresponding electrical equivalent circuit based on the FDTD method is formulated. The coupling between the two problems is incorporated into the heat generation term $\dot{Q}_{\mathrm{g,l}}$, representing Joule losses on the conducting layers, that is proportional to the square of the conductor current I_k. Therefore, given the conductor resistance R, current at all times for each segment is translated into a heat generation event by

$$\dot{Q}_{\mathrm{g,l}} = I^2_k R = I_k(V_{k+1} - V_k). \tag{16}$$

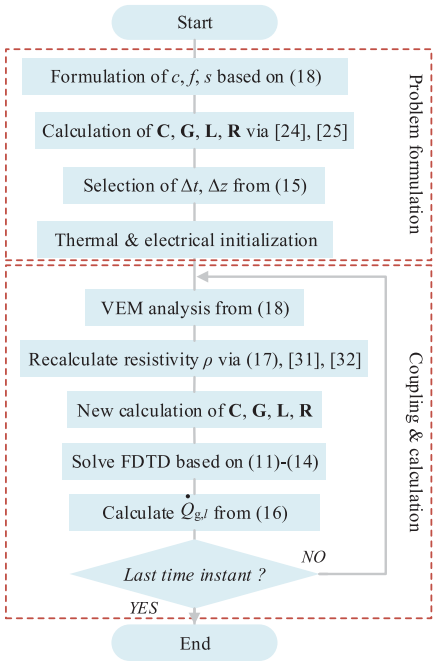

Fig. 2. Flowchart for the electro-thermal coupling process.

On the other hand, the resistivity of most materials changes with temperature [27]. In the case of conventional conductors and insignificant temperature variations, a linear approximation is typically used

$$\rho(T) = \rho_0[1 + \alpha(T - T_0)] = \rho_0 \frac{T_{\rm cr} + T}{T_{\rm cr} + T_0} \qquad (17)$$

where α is the temperature coefficient of resistivity, $-T_{\rm cr}$ is the critical temperature at which resistivity becomes zero, T_0 is a reference temperature, and ρ_0 is the resistivity at temperature T_0. For superconductors, resistivity is extremely low, i.e., in the range of $10^{-12}\,\Omega$m or less, and increases sharply to levels of $10^{-6}\,\Omega$m in case any of the critical conditions (temperature, current density, magnetic field) is exceeded [28]. The nonlinear characteristics of the superconductor were addressed by considering a linear approximation of the areas before and after the point critical conditions occur.

Equations (16) and (17) represent a bidirectional coupling, since current is translated into heat generation, while temperature variations lead to changes on the material resistivity. The coupling is summarized in the flowchart shown in Fig. 2.

V. Case Study

The cable geometry examined is illustrated in Fig. 3 and is based on [4], which is a simplification of the configuration presented in [29] and [30].

Yttrium barium copper oxide (YBCO) is considered as the superconductor, while polypropylene laminated paper (PPLP) and liquid nitrogen (LN_2) are used for insulation and cooling purposes, respectively. Note that the superconducting tape is formulated as a homogeneous medium describing all tape layers. The cable armor and the cryogenic enclosure pipe are made of stainless steel due to the low temperatures, whereas the outside

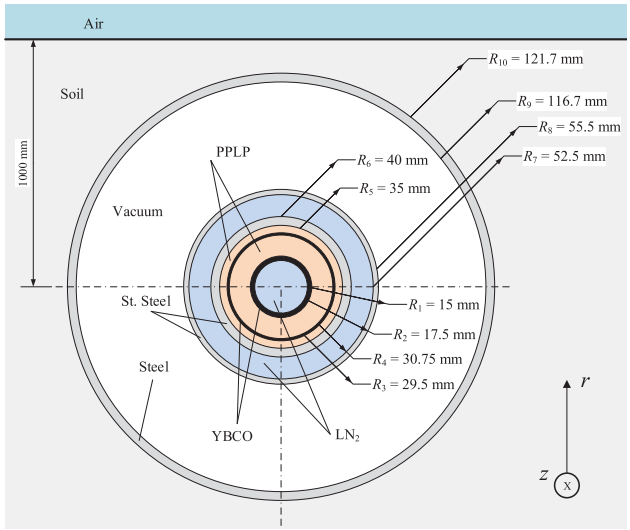

Fig. 3. HTS cable cross section.

TABLE I
Material Properties and Initial Conditions

Material	k (W/mK)	ρ (kg/m^3)	c_v (J/kgK)	c_p (J/kgK)	$T_{\rm init}$ (K)
LN_2 (1,7)	0.026	808	742	1040	72
YBCO (2,4)	208.45	8800	300	–	72
PPLP (3,5)	0.05	946	600	–	72
St. Steel (6,8)	9.4	7600	200	–	72
Steel (10)	16	7800	500	–	299

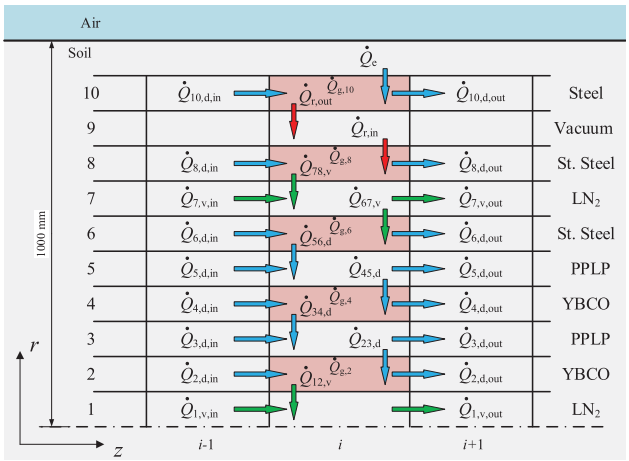

Fig. 4. Heat transfer and volume element discretization.

cable pipe is made of steel. Details on the material properties as well as on the initial conditions $T_{\rm init}$ are given in Table I. The relative permeability of all materials is 1.0, while the insulation relative permittivity of the superconductors and the outer three metallic layers are 2.5 and 1.0, respectively. Lastly, soil resistivity equals $100\,\Omega$m, whereas thermal contact resistances were not considered.

In Fig. 4, heat transfer reference directions are represented by arrows between consecutive VEs on both r and z directions.

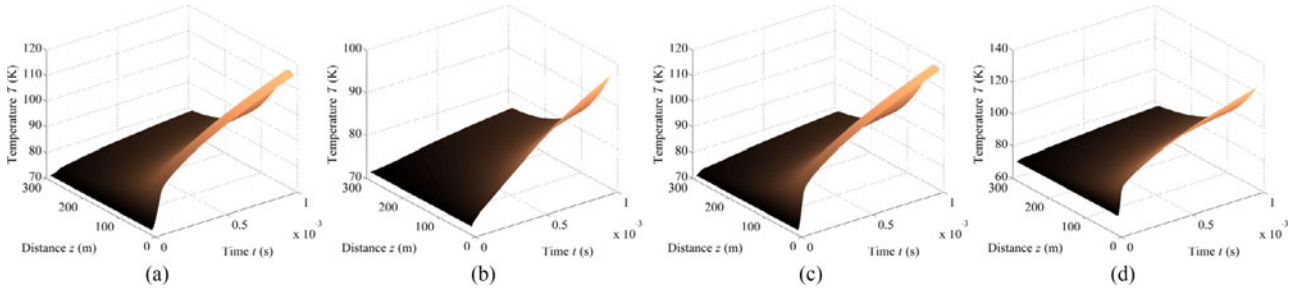

Fig. 5. Temperature distribution of inner and outer YBCO temperature in the case of short-circuit transient scenarios.

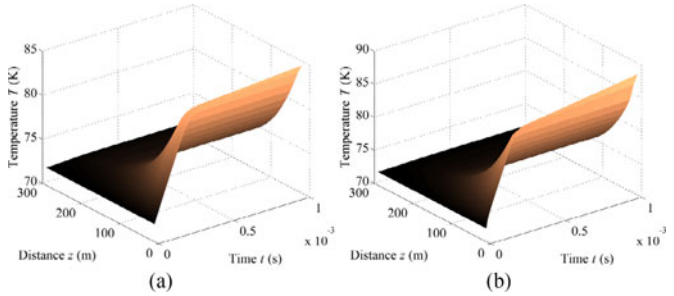

Fig. 6. Temperature distribution in the case of energization.

Heat transfer by conduction, convection, and radiation is represented by blue, green, and red color arrows, respectively.

For the HTS cable cross section and the heat transfer representation illustrated in Figs. 3 and 4, respectively, PDEs that represent the application of the first law of thermodynamics are derived for the ith VE of all layers. Nine PDEs are formulated, since for the perfect vacuum layer no PDE is considered. All PDEs are expressed in the form of (1), in which on the left-hand side of the equation is the coupling term c, whereas the right-hand side contains the flux f and source s terms. Heat transfer on the z axis, i.e., $\dot{Q}^i_{l,\mathrm{d,in}}$ and $\dot{Q}^i_{l,\mathrm{d,out}}$, represents the flux term f. Heat transfer on the r axis, i.e., $\dot{Q}^i_{l_1 l_2,\mathrm{d}}$, $\dot{Q}^i_{\mathrm{r,in}}$, $\dot{Q}^i_{\mathrm{r,out}}$, and $\dot{Q}_{\mathrm{e}}$, represents the source term s. $\dot{Q}_{\mathrm{e}}$ is the amount of heat exchange by conduction from the environment. Finally, heat generation on conductors, expressed as $\dot{Q}_{\mathrm{g,l}}$, is also part of the source term s and embodies the coupling process expressed in Section IV. For brevity, PDE expressing only the first cable layer (inner LN_2 channel) is presented in (18), whereas the remaining ones are defined in detailed in [4]

$$\underbrace{\left(c_{v_{\mathrm{LN}_2}}\,\rho_{\mathrm{LN}_2}\,A_{r,1}\Delta z^i\right)}_{\text{coupling } c}\frac{\partial T^i_1}{\partial t}=\underbrace{\dot{Q}^i_{1,\mathrm{v,in}}-\dot{Q}^i_{1,\mathrm{v,out}}}_{\text{flux } f}+\underbrace{\dot{Q}_{12,\mathrm{v}}}_{\text{source } s}. \tag{18}$$

Considering the electrical formulation, the cross section presented in Fig. 3 consists of five metallic layers; therefore, matrices $\mathbf{C}$, $\mathbf{G}$, $\mathbf{L}$, and $\mathbf{R}$ are of order 5×5. Although the cable is buried, the electromagnetic field propagation velocity approaches the speed of light c, due to the vacuum layer enclosure.

For the electro-thermal coupling part, the special characteristic of the superconductors temperature-dependent resistivity is considered, based on [31]. YBCO resistivity is considerably low, but after the critical temperature of 92 K the material becomes rapidly resistive. This is of crucial importance, since exceeding the critical temperature is translated on a rapid increase of the HTS resistivity, leading to sharp heat generation increase, accordingly. For the steel and stainless steel layers, data from [32] are used.

Regarding the discretization and time-efficiency of the proposed model, 30 VEs are considered for a 300-m cable, i.e., Δz equals 10 m. For the time discretization, the computational burden is significantly affected by the CFL condition presented in (15); therefore, for a simulation duration of 1 ms, Δt equals 3.33×10^{-8} s to be able to accurately capture the transient phenomena. Although a smaller Δz could be selected to capture local quenches or similar events, this would lead to increased simulation duration. In this context, in the proposed methodology, nonuniform discretization in areas of high interest with dense discretization can be adopted, while others can be divided into less segments. For the given discretization setup, the computational burden is 85 h, using an Intel Core i7-5500U, 2.4 GHz, RAM 8 GB personal computer, and MATLAB implementation.

VI. Results

A series of scenarios are examined in order to calculate the temperature increase on HTS cable layers under transients conditions. More specifically, short-circuits, cable energization as well as lightning surges are examined.

A. Short-Circuits

A core-to-ground short-circuit (C2G-SC) and a core-to-sheath short-circuit (C2S-SC) are investigated. A dc voltage source of ± 50 kV is applied on the superconductors, whereas all remaining metallic layers are grounded at both cable ends. In the case of C2G-SC scenario, the cable core (inner YBCO) at the receiving end is short-circuited to ground, while in the case of C2S-SC scenario, the cable core and sheath (inner and outer YBCO) at the receiving end are short-circuited with each other. Results considering the thermal response of the cable system are summarized in Fig. 5. Temperature distribution for only the inner and outer YBCO layers are presented, since temperature increase in all other layers is negligible, i.e., lower than 1 K for the considered simulation period. Fig. 5(a) and (b) indicates

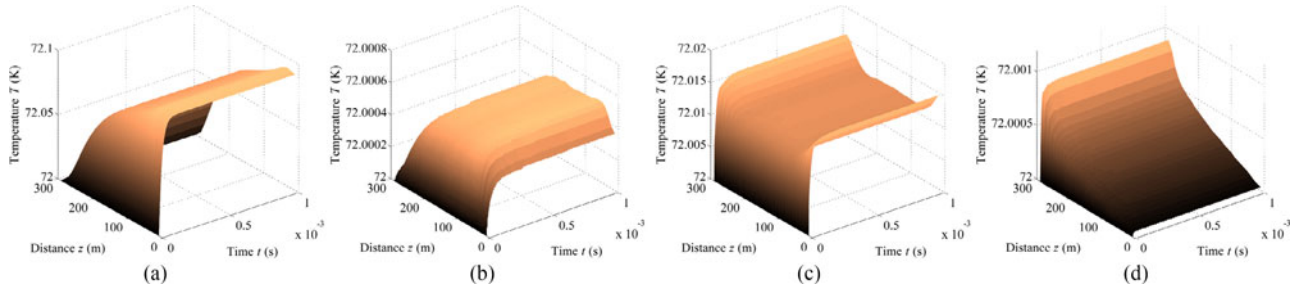

Fig. 7. Temperature distribution of inner and outer YBCO temperature in the case of LI transient scenarios.

that in the case of C2G-SC, temperature on both YBCO layers exceeds the critical temperature of 92 K; therefore, the cable is quenching. The temperature of the inner YBCO layer is mostly affected, since it is short-circuited. Similarly, Fig. 5(c) and (d) corresponds to the C2S-SC setup. This SC scenario is more severe and the temperature increase is higher, exceeding even 130 K. Increase on the outer YBCO layer is evident, since this layer is at a greater radius distance from the (LN_2) channels than the inner one. Consequently, the temperature increase on an YBCO layer depends on the layer's distance from coolant, the environment as well as on the subjected to the fault conductor.

B. Energization

The dc voltage source of ± 50 kV is applied as a step source on the superconductors at the sending end. The temperature of all superconducting materials is already 72 K and, as seen in Fig. 6, a temperature increase of 10–15 K is observed. Although this increase does not put the superconducting state at risk, thermal initialization at temperatures lower than 72 K might be necessary for other setups.

C. Lightning Surges

Lightning surges are simulated by applying a lightning impulse (LI) 1.2/50 μs double-exponential voltage source with a peak of 195 kV at the cable sending end. This peak value is selected as a worst case scenario, based on [33]. Both off-load and on-load condition cases are considered. In the latter, a resistive load equal to 25 Ω is connected to the HTS receiving end. In Fig. 7, the temperature distribution over space and time for the inner and outer YBCO layers is presented. Fig. 7(a) and (b) corresponds to the off-load case, while Fig. 7(c) and (d) to the respective on-load scenario. Although the lightning surge is abrupt, a temperature increase up to 0.1 K at the inner YBCO layer is observed. Accordingly, temperature increase in all other layers, including outer YBCO layer, is insignificant. Finally, the applied voltage at the sending end of inner YBCO, V_{S1}, as well as the voltage response for both YBCO layers at the receiving end, V_{R1} and V_{R2}, are illustrated in Fig. 8, for the off-load case.

Note that surge arresters are not considered as well as corresponding cable physical properties such as dielectric breakdown strength are not included in the analysis as an attempt to focus particularly on the HTS cable modeling and performance and to examine the worst case scenario setup.

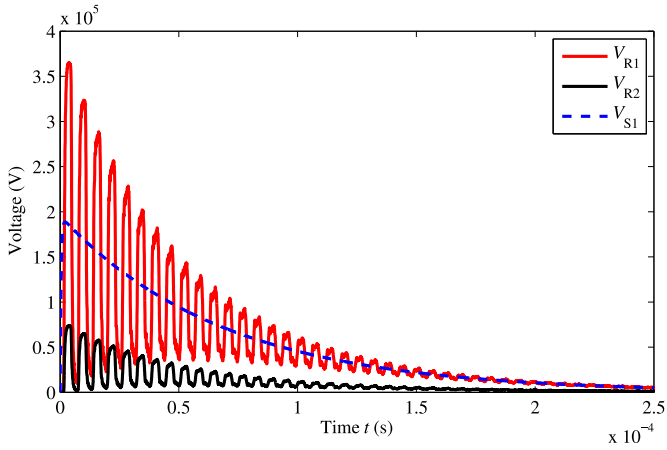

Fig. 8. Voltage response on both YBCO layers for LI off-load.

VII. Conclusion

In this paper, a detailed mathematical formulation regarding the electro-thermal modeling of HTS cables is presented, combined with an efficient numerical solution. Simultaneous discretization over space and time based on the FDTD and VEM techniques is implemented and combined with a time-efficient solver to constitute an accurate simulation tool in order to systematically investigate the coupled electro-thermal behavior of HTS cables under transient conditions.

The proposed method is a useful tool to identify a secure framework, within safe operation of superconducting equipment is ensured, avoiding quenching or severe damage. A series of energization and intense transient scenarios are investigated in order to clarify how temperature distribution at all cable layers is affected. The proposed approach can be applied on any cable configuration given that necessary thermal and electrical data as well as appropriate initializations are provided.

Due to the absence of experimental results and coupled electro-thermal models for HTS cable configurations, the validity of the proposed model can be based on the reliability of the VEM [4], [17], [18], [22], and FDTD [34], applied for the analysis of the thermal and electrical problems, individually or in different types of cable configurations. Moreover, comparisons of the calculated results with [17], [18], [22], and [14]–[16], respectively, indicate that the proposed model can be used to analyze the electro-thermal behavior of HTS cables for varying time and space under different operating conditions.

Conclusions to the actual design and fabrication of an HTS cable are listed as follows.

1) In case of short-circuits, the temperature increase along the HTS cable is significant and most probably lead to quenching and overall equipment deterioration.
2) In case of cable energization, a temperature increase along the HTS cable is observed; however, it is not enough to cause damages to the equipment.
3) In case of lightning surges, temperature increase along the HTS cable is negligible due to the short duration of the phenomenon.

For the future research, assessing the impact of thermal contact resistances on the thermal part of the analysis and addressing the non-linear characteristic of the superconductor in alternative ways are considered.

REFERENCES

[1] N. Flourentzou, V. G. Agelidis, and G. D. Demetriades, "VSC-based HVDC power transmission systems: An overview," *IEEE Trans. Power Electron.*, vol. 24, no. 3, pp. 592–602, Mar. 2009.

[2] J. G. Bednorz and K. A. Muller, "Possible high Tc superconductivity in the Ba-La-Cu-O system," *Zeitschrift für Physik B: Condensed Matter*, vol. 64, pp. 189–193, Apr. 1986.

[3] G. Venkataramanan and B. K. Johnson, "A superconducting DC transmission system based on VSC transmission technologies," *IEEE Trans. Appl. Supercond.*, vol. 13, no. 2, pp. 1922–1925, Jun. 2003.

[4] D. I. Doukas, A. I. Chrysochos, T. A. Papadopoulos, D. P. Labridis, L. Harnefors, and G. Velotto, "Volume element method for thermal analysis of superconducting DC transmission cable," *IEEE Trans. Appl. Supercond.*, vol. 27, no. 4, Jun. 2017, Art. no. 5400608.

[5] D. I. Doukas, Z. D. Blatsi, A. N. Milioudis, D. P. Labridis, L. Harnefors, and G. Velotto, "Damping of electromagnetic transients in a superconducting VSC transmission system," in *Proc. IEEE PowerTech Eindhoven*, Jun. 2015, pp. 1–6.

[6] F. Grilli, E. Pardo, A. Stenvall, D. N. Nguyen, W. Yuan, and F. Gmry, "Computation of losses in HTS under the action of varying magnetic fields and currents," *IEEE Trans. Appl. Supercond.*, vol. 24, no. 1, pp. 78–110, Feb. 2014.

[7] F. Grilli, "Numerical modeling of HTS applications," *IEEE Trans. Appl. Supercond.*, vol. 26, no. 3, Apr. 2016, Art. no. 0500408.

[8] L. Bottura, "Thermal, hydraulic, and electromagnetic modeling of superconducting magnet systems," *IEEE Trans. Appl. Supercond.*, vol. 26, no. 3, Apr. 2016, Art. no. 4901807.

[9] Z. Zhou *et al.*, "Magnetic-thermal coupling analysis of the cold dielectric high temperature superconducting cable," *IEEE Trans. Appl. Supercond.*, vol. 23, no. 3, Jun. 2013, Art no. 5400404.

[10] M. Breschi, M. Casali, L. Cavallucci, G. D. Marzi, and G. Tomassetti, "Electrothermal analysis of a twisted stacked YBCO cable-in-conduit conductor," *IEEE Trans. Appl. Supercond.*, vol. 25, no. 3, Jun. 2015, Art. no. 4800505.

[11] M. Watanabe *et al.*, "Thermo-mechanical properties of a 66 kV superconducting power cable system," *IEEE Trans. Appl. Supercond.*, vol. 13, no. 2, pp. 1956–1959, Jun. 2003.

[12] R. Zanino, F. Bellina, P. L. Ribani, and L. S. Richard, "Coupled thermal-hydraulic/electromagnetic analysis and interpretation of the test results of the ITER TFPRO2 OST1 conductor," *IEEE Trans. Appl. Supercond.*, vol. 19, no. 3, pp. 1483–1487, Jun. 2009.

[13] G. S. Lee *et al.*, "Monitoring electrical and thermal characteristics of HTS cable systems via time-frequency domain reflectometry," *IEEE Trans. Appl. Supercond.*, vol. 27, no. 4, Jun. 2017, Art. no. 9000605.

[14] C. Pallem, P. Chowdhuri, J. A. Demko, and M. J. Gouge, "Parametric effects on the transient voltage performance of a dc superconducting cable," *IEEE Trans. Appl. Supercond.*, vol. 16, no. 1, pp. 31–37, Mar. 2006.

[15] P. Chowdhuri, C. Pallem, J. A. Demko, and M. J. Gouge, "Analysis on the transient voltage performance of a DC superconducting cable," *IEEE Trans. Appl. Supercond.*, vol. 16, no. 1, pp. 21–30, Mar. 2006.

[16] J. G. Kim, M. A. Salmani, L. Graber, C. H. Kim, and S. V. Pamidi, "Electrical characteristics and transient analysis of HTS DC power cables for shipboard application," in *Proc. 2015 IEEE Elect. Ship Technol. Symp.,*Jun. 2015, pp. 376–381.

[17] N. G. Suttell, J. V. C. Vargas, and J. C. Ordonez, "Transient thermal analysis of HTS DC cables cooled with gaseous helium using a volume element method transactions on applied superconductivity," *IEEE Trans. Appl. Supercond.*, vol. 27, no. 4, Jun. 2017, Art. no. 4800505.

[18] N. G. Suttell, C. H. Kim, S. V. Pamidi, and J. C. Ordonez, "Transient cryogenic thermal modeling of HTS cable systems cooled with gaseous Helium transactions on applied superconductivity," *IEEE Trans. Appl. Supercond.*, vol. 27, no. 4, Jun. 2017, Art. no. 5401005.

[19] Y. Yang, I. Falorio, J. Pelegrin, E. A. Young, and A. Ballarino, "Transient thermoelectrical behavior of MgB2 cables in the superconducting links for the high luminosity upgrade of the LHC," *IEEE Trans. Appl. Supercond.*, vol. 27, no. 4, Jun. 2017, Art. no. 4801505.

[20] R. D. Skeel and M. Berzins, "A method for the spatial discretization of parabolic equations in one space variable," *SIAM J. Sci. Stat. Comput.*, vol. 11, no. 1, pp. 1–32, 1990.

[21] MATLAB, version 8.2.0.701 (R2013b). Natick, MA, USA: MathWorks Inc., 2013.

[22] J. A. Souza, J. C. Ordonez, R. Hovsapian, and J. V. C. Vargas, "Thermal modeling of helium cooled high-temperature superconducting DC transmission cable," *IEEE Trans. Appl. Supercond.*, vol. 21, no. 3, pp. 947–952, Jun. 2011.

[23] C. R. Paul, *Analysis of multiconductor transmission lines*. New York, NY, USA: Wiley, 2008.

[24] A. Ametani, "A general formulation of impedance and admittance of cables," *IEEE Trans. Power App. Syst.*, vol. PAS-99, no. 3, pp. 902–910, May 1980.

[25] A. I. Chrysochos, T. A. Papadopoulos, and G. K. Papagiannis, "Rigorous calculation method for resonance frequencies in transmission line responses," *IET Gener. Transmiss. Distrib.*, vol. 9, no. 8, pp. 767–778, Aug. 2015.

[26] R. Courant, K. Friedrichs, and H. Lewy, "Über die partiellen differenzengleichungen der mathematischen physik," *Mathematische Annalen*, vol. 100, no. 1, pp. 32–74, 1928.

[27] M. R. Ward, *Electrical Engineering Science*. New York, NY, USA: McGraw-Hill, 1971.

[28] C. Rey, *Superconductors in the Power Grid: Materials and Applications*. Amsterdam, The Netherlands: Elsevier, 2015.

[29] "Program on technology innovation: A superconducting DC cable," *EPRI, Palo Alto, CA, USA, Rep.* 1020458, Dec. 2009.

[30] "Program on technology innovation: Transient response of a superconducting DC long length cable system using voltage source converters," EPRI, Palo Alto, CA, USA, Rep. 1020339, Dec. 2009.

[31] J. Jung and M. Abdelhadi, "Temperature dependence of in-plane resistivity of (YBCO)," Dept. Physics, Univ. Alberta, Edmonton, Alberta, Canada, Tech. Rep., Jan. 2005.

[32] P. Duthil, "Material properties at low temperature," in *Proc. CAS-CERN Accelerator School: Supercond. Accelerators*, 2015, pp. 77–95.

[33] *Insulation Co-Ordination—Part 1: Definitions, Principles and Rules*," IEC 60071-1:2006, 2006.

[34] C. G. Kaloudas, A. I. Chrysochos, and G. K. Papagiannis, "FDTD analysis of multiphase power cable systems using distributed constant parameters," in *Proc. MedPower*, Nov. 2014, pp. 1–8.

Dimitrios I. Doukas (S'13–M'17) received the Dipl.-Eng in electrical and computer engineering from the Aristotle University of Thessaloniki, Greece, in 2009, the M.Sc. degree in sustainable energy systems from the University of Edinburgh, Edinburgh, U.K., in 2011 and the Ph.D. in electrical and computer engineering from the Aristotle University of Thessaloniki, Greece, in 2017.

From 2011 to 2013, he was with ABB Corporate Research, Västerås, Sweden. His research interests are applied superconductivity, energy storage, and power system analysis and control.

Andreas I. Chrysochos (S'08–M'16) received the Dipl.-Eng and Ph.D. degrees in electrical and computer engineering from the Aristotle University of Thessaloniki, Greece, in 2009 and 2015, respectively.

He is currently a Postdoc Researcher in the Department of Electrical and Computer Engineering, Democritus University of Thrace, Xanthi, Greece, and also the R&D Senior Engineer in Cablel Hellenic Cables S.A., Viohalco Group, Marousi, Greece. His research interests include power systems modeling, computation of electromagnetic transients, and PLC. He has been a scholar of the Alexander S. Onassis Public Benefit Foundation (2012–2015, 2016–2017).

Theofilos A. Papadopoulos (S'01–M'09) received the Dipl.-Eng and Ph.D. degrees in electrical and computer engineering from the Aristotle University of Thessaloniki, Greece, in 2003 and 2008, respectively.

He is currently an Associate Professor in the Power Systems Laboratory, Department of Electrical and Computer Engineering, Democritus University of Thrace, Komotini, Greece. His research interests include power systems modeling, PLC, and computation of electromagnetic transients.

Dr. Papadopoulos received the Basil Papadias Award at the IEEE PowerTech'07 Conference.

Dimitris P. Labridis (S'88–M'90–SM'00) received the Dipl.-Eng and Ph.D. degrees in electrical and computer engineering from the Aristotle University of Thessaloniki, Greece, in 1981 and 1989, respectively.

Since 1986 he has been working as a Professor with the Department of Electrical Engineering, Aristotle University of Thessaloniki. His research interests include power system analysis with a special emphasis on the simulation of transmission and distribution systems, smart grids, distributed energy resources, power line communications, coupled electromagnetic and thermal field analysis, interference of power transmission and distribution lines, artificial intelligence applications in power systems, and applied superconductivity.

Lennart Harnefors (S'93–M'97–SM'07–F'17) was born in 1968 in Eskilstuna, Sweden. He received the M.Sc., Licentiate, and Ph.D. degrees in electrical engineering from the Royal Institute of Technology (KTH), Stockholm, Sweden, in 1993, 1995, and 1997, respectively, and the Docent (D.Sc.) degree in industrial automation from Lund University, Lund, Sweden, in 2000.

He is currently a Senior Principal Scientist with Corporate Research, Västerås, Sweden. Since 2011, he has also been a part-time Adjunct Professor of power electronics with the KTH. During 1994–2005, he was with Mälardalen University, Västerås, Sweden, from 2001 as a Professor of electrical engineering. During 2001–2005, he was, in addition, a part-time Visiting Professor of electrical drives with Chalmers University of Technology, Gothenburg, Sweden. Since 2005, he has been with ABB Power Systems, where he has served in various capacities with the Grid Systems/HVDC business unit, Ludvika, Sweden, from 2005 to 2012. His research interests include control and dynamic analysis of power electronic systems, particularly grid-connected converters, ac drives, and wide-bandgap-transistor switching circuits.

Dr. Harnefors is an Associate Editor of the IEEE TRANSACTIONS ON INDUSTRIAL ELECTRONICS and *IET Electric Power Applications*.

Giovanni Velotto was born in Naples, Italy, on October 8, 1976. He received the Laurea degree in electrical engineering and the Ph.D. degree in power systems engineering from the Universit degli Studi di Napoli Federico II, Naples, Italy, in 2003 and 2007, respectively.

He is currently a Senior Scientist with ABB Corporate Research, Västerås, Sweden. His main research interests include the stochastic analysis and control of electrical power systems.